Redefined Block-Lifting-based Filter Banks with Efficient Reversible Nonexpansive Convolution

Taizo Suzuki, *Senior Member, IEEE*, Naoki Tanaka, Hiroyuki Kudo, *Member, IEEE*

***Abstract*—This study redefines a block-lifting structure of M-channel ($M \in \mathbb{N}$, $M \geq 2$) filter banks and proposes an efficient reversible nonexpansive convolution at the boundaries for lossy-to-lossless image coding. The previous studies left two problems. One is that the conventional lifting-based FBs are restricted to having equal analysis/synthesis filter lengths. We derive block-lifting-based FBs (BLFBs) with not only equal analysis/synthesis filter lengths but also the longer synthesis filter lengths than those of the analysis banks. The other problem is that the conventional lifting-based FBs without the linear-phase (LP) property, such as BLFBs, cannot implement the conventional smooth nonexpansive convolution at the boundaries because of the rounding error in each lifting. We solve the boundary problem by using an efficient reversible nonexpansive convolution derived from a nonexpansive convolution for nonlinear-phase FBs with paraunitariness. We show that the redefined BLFBs (ReBLFBs) with the efficient reversible nonexpansive convolution perform well at lossy-to-lossless image coding.**

***Index Terms*—Block-lifting structure, filter bank, filter length, lossy-to-lossless image coding, nonexpansive convolution.**

I. Introduction

IMAGE compression (coding), which is one of the most useful preprocessing technologies of communications, is classified into lossy and lossless. Lossy image coding dramatically compacts the data size of natural images taken by digital cameras and smartphones at the expense of image quality, whereas lossless image coding losslessly compacts the data size of medical, satellite, and art images at the expense of the compression rate; i.e., image quality and compression rate are in a trade-off. To cover all images in a cross-sectoral manner, lossy-to-lossless image coding, which has scalability from lossless to lossy data, has been incorporated in image coding standards such as JPEG 2000 [1] and JPEG XR [2].[1]

The lifting structure [5], that maps integer input signals to integer output signals by performing a rounding operation before the addition in each lifting step, contributes to achieving the lossy-to-lossless image coding. The JPEG 2000 uses 5/3- and 9/7-tap discrete wavelet transforms (DWTs), and their various related works have been presented [6–9]. However, since DWTs, which are considered as two-channel filter banks (FBs), may be limited to design the better transforms because of a few free parameters, many M-channel ($M \in \mathbb{N}$, $M \geq 2$, M is even) lifting-based FBs have been presented in the literature [10–19]. In [11], Tran *et al.* introduced time-domain lapped transforms (TDLTs), which can be directly applied to the JPEG framework. In [14], Tu *et al.* introduced a 4×8 lifting-based hierarchical lapped transform (HLT) for the JPEG XR by extending TDLTs. However, since FBs with linear-phase (LP) property such as TDLT and HLT may be also limited to design the better transforms, several nonlinear-phase FBs have been studied for more efficient image coding. In [17], Iwamura *et al.* presented nonlinear-phase FBs based on a *block-lifting* structure that reduces the rounding error by merging many rounding operations, called block-lifting-based FBs (BLFBs), because the rounding error reduces the coding efficiency. In [18], we generalized the BLFBs; i.e., we allowed the McMillan degree r_k to be $1 \leq r_k < M$ and allowed both even and odd block size. In [19], we presented their 2-D nonseparable structures.[2]

On the other hand, it is known that the analysis banks basis functions (or impulse response) should be short to avoid ringing artifacts around regions with high-frequency components, whereas the synthesis banks should be long and their coefficients should decay to zero smoothly at both ends to avoid blocking artifacts around regions with low-frequency components [23]. Nevertheless, the conventional lifting-based FBs are restricted to having equal analysis/synthesis filter lengths. Moreover, although our previous work [24] allows the traditional smooth nonexpansive convolution, a symmetric extension [25], at the boundaries in lifting-based FBs with a LP property, it does not allow any conventional nonexpansive convolution to be used in M-channel nonlinear-phase cases [24–27] because of the rounding error. In particular, the M-channel nonlinear-phase cases except for $M = 2$ must have a common periodic extension, whose discontinuity at the boundaries yields the annoying artifacts.

This study redefines a block-lifting structure of M-channel FBs for lossy-to-lossless image coding. The redefined BLFBs (ReBLFBs) can derive not only equal analysis/synthesis filter lengths but also the longer synthesis filter lengths than the analysis ones. Also, we produce an efficient reversible nonexpansive convolution unrestricted by the LP property.

T. Suzuki and H. Kudo are with the Faculty of Engineering, Information and Systems, University of Tsukuba, Tsukuba, Ibaraki, 305-8573 Japan (e-mail: {taizo, kudo}@cs.tsukuba.ac.jp).

N. Tanaka is with the Department of Computer Science, University of Tsukuba, Tsukuba, Ibaraki, 305-8573 Japan (e-mail: tanaka@imagelab.cs.tsukuba.ac.jp).

[1]This study focuses on "lossy-to-lossless image coding." Although there are the newer image coding methods with machine learning and neural networks as in [3], [4], which may outperform the traditional transform coding as in this study, they are specialized for only lossy image coding and cannot be applied to lossless image coding.

[2]This study focuses on "transforms for general natural images," i.e., they are basic technologies that can be customized if necessary and widely used. Although there are some newer studies for lossy-to-lossless image coding [20–22], they have proposed more efficient uses of the traditional transforms such as DWTs and the methods for specified images such as medical and hyperspectral image.

A preliminary work of the nonexpansive convolution will be presented in [28], where we discussed only FBs with paraunitariness and equal analysis/synthesis filter lengths. This paper describes the unrestricted case for the characteristics. We show that the ReBLFBs with the nonexpansive convolution perform well at lossy-to-lossless image coding.

The remaining part of this paper is organized as follows. Section II reviews the BLFBs. Section III redefines the BLFBs for a structure embodying the conventional block-lifting structure and proposes an efficient reversible boundary processing. Section IV presents the filter design and the experimental results. Section V concludes this paper.

Notations: $\mathbf{I}$, $\mathbf{J}$, $\mathbf{O}$, $\det(\cdot)$, superscript $\top$, and subscript $[m]$ ($m \in \mathbb{N}$) denote an identity matrix, reversal matrix, zero matrix, determinant of a matrix, transpose of a vector/matrix, and $m \times m$ matrix, respectively. The subscript $[m]$ is omitted if its size is clear.

II. Review and Definition

A. Filter Banks

The polyphase matrix of causal M-channel maximally decimated $(K-1)$th order ($M \times MK$, $K \in \mathbb{N}$) FBs is factorized as follows [29]:

$$\mathbf{E}(z) = \mathbf{E}_{K-1}(z)\mathbf{E}_{K-2}(z)\cdots\mathbf{E}_1(z)\mathbf{X}_0, \tag{1}$$

where the initial block $\mathbf{X}_0$ is an $M \times M$ nonsingular matrix, and $\mathbf{E}_k(z)$ $(1 \le k \le K-1)$ can be factorized into

$$\mathbf{E}_k(z) = \mathbf{I}_{[M]} - \boldsymbol{\mathcal{U}}_k\boldsymbol{\mathcal{V}}_k^\top + z^{-1}\boldsymbol{\mathcal{U}}_k\boldsymbol{\mathcal{V}}_k^\top, \tag{2}$$

where the $M \times r_k$ parameter matrices $\boldsymbol{\mathcal{U}}_k$ and $\boldsymbol{\mathcal{V}}_k$ satisfy

$$\boldsymbol{\mathcal{V}}_k^\top\boldsymbol{\mathcal{U}}_k = \begin{bmatrix} 1 & \times & \cdots & \times \\ 0 & 1 & \ddots & \vdots \\ \vdots & \ddots & \ddots & \times \\ 0 & \cdots & 0 & 1 \end{bmatrix}_{[r_k]} \triangleq \boldsymbol{\mathcal{W}}_k \tag{3}$$

for some integer $1 \le r_k < M$, where $\times$ indicates possibly nonzero elements. Let $\boldsymbol{\mathcal{U}}_k$ and $\boldsymbol{\mathcal{V}}_k$ be

$$\boldsymbol{\mathcal{U}}_k = \begin{bmatrix} \mathbf{u}_{k0} \\ \mathbf{u}_{k1} \end{bmatrix} \tag{4}$$

$$\boldsymbol{\mathcal{V}}_k = \begin{bmatrix} \mathbf{v}_{k0} \\ \mathbf{v}_{k1} \end{bmatrix}, \tag{5}$$

where $\mathbf{u}_{k0}$ and $\mathbf{v}_{k0}$ are $q_k \times r_k$ ($q_k = M - r_k$) matrices and $\mathbf{u}_{k1}$ and $\mathbf{v}_{k1}$ are $r_k \times r_k$ square matrices, respectively, for later discussion. The synthesis polyphase matrix $\mathbf{R}(z)$ is given by

$$\mathbf{R}(z) = \mathbf{X}_0^{-1}\mathbf{E}_1^{-1}(z)\cdots\mathbf{E}_{K-1}^{-1}(z),$$

which is anticausal as a result of (3) and satisfies $\mathbf{R}(z)\mathbf{E}(z) = \mathbf{I}$ for perfect reconstruction [30]. Since the rank of $\boldsymbol{\mathcal{W}}_k$ in (3) is r_k, the McMillan degree of $\mathbf{E}_k(z)$, as in (2), is r_k and the matrix $\mathbf{E}_k(z)$ is a *degree-r_k* building block. If $r_k = \frac{M}{2}$ (M is even), $\lceil \frac{M}{2} \rceil$ (M and k are odd), or $\lfloor \frac{M}{2} \rfloor$ (M is odd and k is even) [31], the $\mathbf{E}_k(z)$ is an *order*-1 building block. K must be odd when M is odd.

Almost all studies impose the restriction $\boldsymbol{\mathcal{W}}_k = \mathbf{I}_{[r_k]}$ that guarantees equal filter lengths in analysis/synthesis banks. In addition, when $\boldsymbol{\mathcal{V}}_k = \boldsymbol{\mathcal{U}}_k$, the FBs are paraunitary filter banks (PUFBs) and the others are biorthogonal FBs (BOFBs). This study eases the restriction on the filter lengths and paraunitariness, i.e., $\boldsymbol{\mathcal{W}}_k \neq \mathbf{I}_{[r_k]}$, and produces FBs with longer synthesis filter lengths than those of the analysis banks.

B. Block-Lifting-based Filter Banks

The lifting structure [5] is a cascade of elementary matrices, which are identity matrices with one single nonzero off-diagonal element. It preserves reversibility if the rounding operation is performed before the addition in each lifting step. The block-lifting structure [17–19], which is a special class of lifting structure, achieves good lossy-to-lossless image coding because it reduces the rounding error, which adversely affects coding efficiency, by merging many rounding operations. Through the restriction $\boldsymbol{\mathcal{W}}_k = \mathbf{I}_{[r_k]}$, the block-lifting-based building block $\mathbf{E}_k(z)$ is expressed as

$$\mathbf{E}_k(z) = \mathfrak{L}_k^{-1}\mathfrak{U}_k\boldsymbol{\Lambda}_k(z)\mathfrak{U}_k^{-1}\mathfrak{L}_k, \tag{6}$$

where

$$\mathfrak{L}_k = \begin{bmatrix} \mathbf{I}_{[q_k]} & \mathbf{O} \\ \mathbf{v}_{k1}^{-\top}\mathbf{v}_{k0}^\top & \mathbf{I}_{[r_k]} \end{bmatrix} \tag{7}$$

$$\mathfrak{U}_k = \begin{bmatrix} \mathbf{I}_{[q_k]} & \mathbf{u}_{k0}\mathbf{v}_{k1}^\top \\ \mathbf{O} & \mathbf{I}_{[r_k]} \end{bmatrix}. \tag{8}$$

The inverse building block $\mathbf{E}_k^{-1}(z)$ is obtained as follows:

$$\mathbf{E}_k^{-1}(z) = \mathfrak{L}_k^{-1}\mathfrak{U}_k\boldsymbol{\Lambda}_k^{-1}(z)\mathfrak{U}_k^{-1}\mathfrak{L}_k. \tag{9}$$

Note that the initial block $\mathbf{X}_0$ is restricted to $|\det(\mathbf{X}_0)| = d$ ($d \in \mathbb{N}$) for the purpose of making a lifting factorization. It can be factorized into non block-lifting structures, e.g., the single-row elementary reversible matrices (SERMs) presented in [10]. In addition, lifting-based FBs without the LP property, such as BLFBs, cannot directly use the conventional smooth nonexpansive convolution [24–27] at the boundaries because of the rounding error. A periodic extension, which is commonly used for boundary processing in the M-channel nonlinear-phase cases except for $M = 2$, causes annoying boundary artifacts in low-bit compression because of the discontinuity.

III. Redefined Block-Lifting-based Filter Banks with Reversible Nonexpansive Convolution

A. Redefined Block-Lifting Structure for Filter Banks

Theorem: By not setting the restriction $\boldsymbol{\mathcal{W}}_k = \mathbf{I}_{[r_k]}$ that is used in [18], we can redefine a building block $\mathbf{E}_k(z)$ as a more generalized block-lifting structure as follows (Fig. 1):

$$\mathbf{E}_k(z) = \mathfrak{L}_k^{-1}\mathfrak{W}_k(z)\mathfrak{U}_k\boldsymbol{\Lambda}_k(z)\mathfrak{U}_k^{-1}\mathfrak{L}_k, \tag{10}$$

where

$$\mathfrak{W}_k(z) = \begin{bmatrix} \mathbf{I}_{[q_k]} & \mathbf{O} \\ \mathbf{O} & \widetilde{\boldsymbol{\mathcal{W}}}_k \end{bmatrix} \begin{bmatrix} \mathbf{I}_{[q_k]} & \mathbf{O} \\ \mathbf{O} & \mathbf{I}_{[r_k]} + z\left(\widetilde{\boldsymbol{\mathcal{W}}}_k^{-1} - \mathbf{I}_{[r_k]}\right) \end{bmatrix} \tag{11}$$

$$\widetilde{\boldsymbol{\mathcal{W}}}_k = \mathbf{v}_{k1}^{-\top}\boldsymbol{\mathcal{W}}_k\mathbf{v}_{k1}^\top. \tag{12}$$

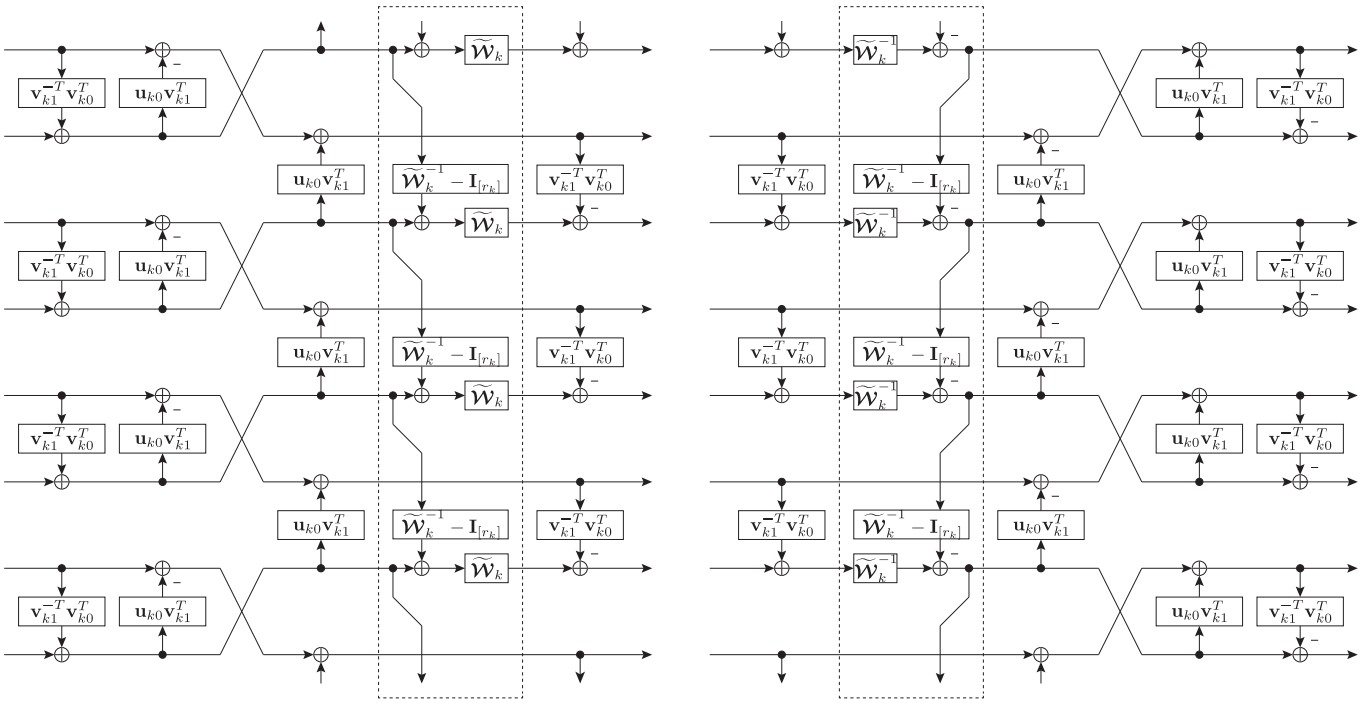

Fig. 1. Building block of ReBLFB (areas enclosed by dashed lines mean the new part, and arrows mean $\frac{M}{2} \times \frac{M}{2}$ signals, respectively): (left) analysis bank, (right) synthesis bank.

$\mathfrak{W}_k(z)$ is the new part of the block-lifting structure. The $\widetilde{\mathcal{W}}_k$ in the first term $\mathrm{diag}(\mathbf{I}_{[q_k]}, \widetilde{\mathcal{W}}_k)$ in (11) can be easily factorized into a variety of lifting structures because

$$\det(\widetilde{\mathcal{W}}_k) = \det(\mathbf{v}_{k1}^{-\top}) \cdot \det(\mathcal{W}_k) \cdot \det(\mathbf{v}_{k1}^{\top}) = 1, \quad (13)$$

where

$$\det(\mathcal{W}_k) = 1 \quad \text{and} \quad \det(\mathbf{v}_{k1}^{-\top}) \cdot \det(\mathbf{v}_{k1}^{\top}) = 1, \quad (14)$$

which is a sufficient condition for the purpose of making a lifting factorization. The second term $\mathrm{diag}(\mathbf{I}_{[q_k]}, \mathbf{I}_{[r_k]} + z(\widetilde{\mathcal{W}}_k^{-1} - \mathbf{I}_{[r_k]}))$ in (11) can already be considered a lifting structure with a lifting coefficient $z(\widetilde{\mathcal{W}}_k^{-1} - \mathbf{I}_{[r_k]})$. The inverse building block $\mathbf{E}_k^{-1}(z)$ is obtained as follows:

$$\mathbf{E}_k^{-1}(z) = \mathfrak{L}_k^{-1}\mathfrak{U}_k\mathbf{\Lambda}_k^{-1}(z)\mathfrak{U}_k^{-1}\mathfrak{W}_k^{-1}(z)\mathfrak{L}_k, \quad (15)$$

where

$$\mathfrak{W}_k^{-1}(z) = \begin{bmatrix} \mathbf{I}_{[q_k]} & \mathbf{O} \\ \mathbf{O} & \mathbf{I}_{[r_k]} - z\left(\widetilde{\mathcal{W}}_k^{-1} - \mathbf{I}_{[r_k]}\right) \end{bmatrix} \begin{bmatrix} \mathbf{I}_{[q_k]} & \mathbf{O} \\ \mathbf{O} & \widetilde{\mathcal{W}}_k^{-1} \end{bmatrix}. \quad (16)$$

When $\mathcal{W}_k = \mathbf{I}_{[r_k]}$, i.e., $\mathfrak{W}_k(z) = \mathbf{I}_{[M]}$, (10) and (15) are completely equivalent to the conventional building block $\mathbf{E}_k(z)$ and the inverse $\mathbf{E}_k^{-1}(z)$ in [18].

Proof: In accordance with [18], $\mathbf{E}_k(z)$ in (2)-(5) is rewritten as

$$\mathbf{E}_k(z) = \begin{bmatrix} \mathbf{I}_{[q_k]} + \left(z^{-1} - 1\right)\mathbf{u}_{k0}\mathbf{v}_{k0}^{\top} & \left(z^{-1} - 1\right)\mathbf{u}_{k0}\mathbf{v}_{k1}^{\top} \\ \left(z^{-1} - 1\right)\mathbf{u}_{k1}\mathbf{v}_{k0}^{\top} & \mathbf{I}_{[r_k]} + \left(z^{-1} - 1\right)\mathbf{u}_{k1}\mathbf{v}_{k1}^{\top} \end{bmatrix}. \quad (17)$$

The lower block-lifting matrix $\mathfrak{L}_k$ expressed as (7) and its inverse $\mathfrak{L}_k^{-1}$ are respectively multiplied from the left and right sides of $\mathbf{E}_k(z)$ as follows:

$$\mathfrak{L}_k\mathbf{E}_k(z)\mathfrak{L}_k^{-1} = \begin{bmatrix} \mathbf{I}_{[q_k]} & \left(z^{-1} - 1\right)\mathbf{u}_{k0}\mathbf{v}_{k1}^{\top} \\ \mathbf{O} & \mathbf{I}_{[r_k]} + \left(z^{-1} - 1\right)\widetilde{\mathcal{W}}_k \end{bmatrix}. \quad (18)$$

By using the upper block-lifting matrix $\mathfrak{U}_k$ expressed as (8), its inverse $\mathfrak{U}_k^{-1}$, and $\mathbf{\Lambda}_k(z)$, (18) can be further factorized as

$$\mathfrak{L}_k\mathbf{E}_k(z)\mathfrak{L}_k^{-1} = \mathfrak{W}_k\mathfrak{U}_k\mathbf{\Lambda}_k(z)\mathfrak{U}_k^{-1} \triangleq \widetilde{\mathbf{E}}_k(z). \quad (19)$$

Consequently, $\mathbf{E}_k(z)$ can be factorized into the lifting matrices as in (10) because

$$\mathbf{E}_k(z) = \mathfrak{L}_k^{-1}\widetilde{\mathbf{E}}_k(z)\mathfrak{L}_k = \mathfrak{L}_k^{-1}\mathfrak{W}_k(z)\mathfrak{U}_k\mathbf{\Lambda}_k(z)\mathfrak{U}_k^{-1}\mathfrak{L}_k. \quad (20)$$

B. Reversible Nonexpansive Convolution for Lifting-based Filter Banks

This subsection uses the following FB:

$$\mathbf{E}(z) = \mathbf{X}_{K-1}\mathbf{\Lambda}_{K-1}(z)\cdots\mathbf{X}_1\mathbf{\Lambda}_1(z)\mathbf{X}_0, \quad (21)$$

where $\mathbf{X}_k$ is a nonsingular matrix, M is even, and $r_k = \frac{M}{2}$ for simplicity. The top images of Figs. 2 and 3 show the upper boundary processing of the FBs when $K = 2$ and 3. They mean that $L = \frac{(K-1)M}{2}$ extra signals have to be extended at each boundary. To obtain smooth signals, the extra signals are commonly extended by using an $L \times L$ extension matrix:

$$\mathcal{E}_{[L]} = \mathbf{J}_{[L]}; \quad (22)$$

i.e., it is a symmetric extension [25]. We derive an efficient reversible nonexpansive convolution for lifting-based FBs from a nonexpansive convolution for PUFBs [26] as follows:

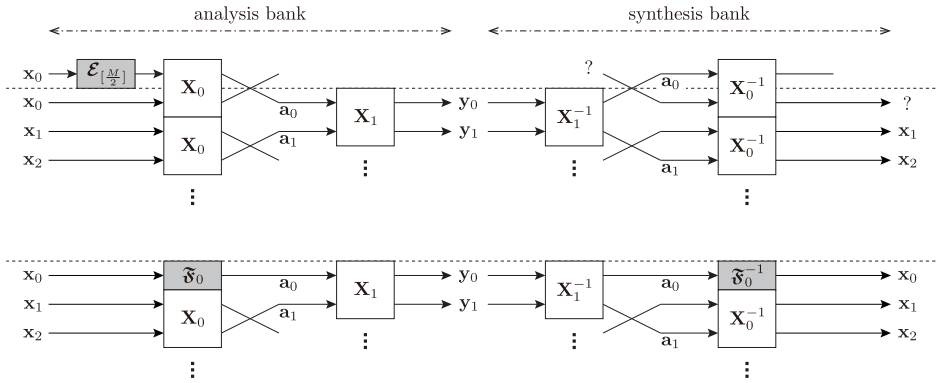

Fig. 2. Upper boundary processing of $M \times 2M$ FBs (dashed lines and arrows indicate the upper boundary and $\frac{M}{2} \times \frac{M}{2}$ signals, respectively): (top) simple signal extension; (right) nonexpansive convolution.

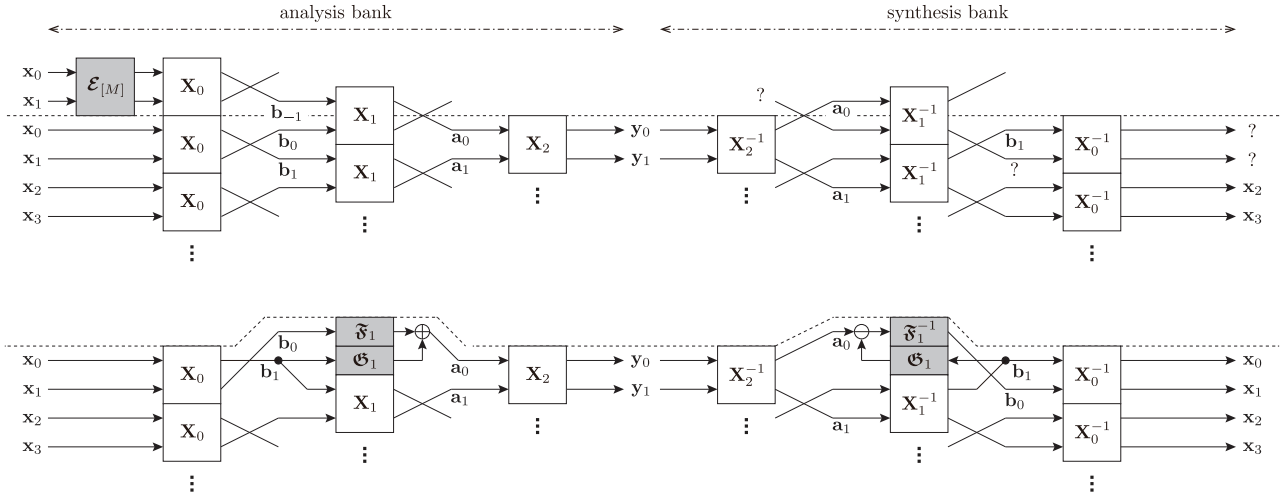

Fig. 3. Upper boundary processing of $M \times 3M$ FBs (dashed lines and arrows indicate the upper boundary and $\frac{M}{2} \times \frac{M}{2}$ signals, respectively): (top) simple signal extension; (right) nonexpansive convolution.

1) Remove the paraunitariness restriction.
2) Use an arbitrary extension matrix $\boldsymbol{\mathcal{E}}_{[L]}$, not a symmetric extension matrix $\mathbf{J}_{[L]}$.
3) Restrict the determinant of the resulting boundary matrix $\mathfrak{F}_k$ to $|\det(\mathfrak{F}_k)| = d$ ($d \in \mathbb{N}$) for the purpose of making a lifting factorization [10].

Here, we have a nonexpansive problem because the signals transmitted to the synthesis bank should only be the output $\mathbf{y}_n$ ($n \in \mathbb{N}$). This subsection presents a reconstruction method at the synthesis bank without any extra signal; i.e., the input signal $\mathbf{x}_n$ is reconstructed from only the output signal $\mathbf{y}_n$. To facilitate the discussion, let an $M \times M$ matrix $\mathbf{M}$ be

$$\mathbf{M} = \begin{bmatrix} [\mathbf{M}]_\alpha & [\mathbf{M}]_\beta \\ [\mathbf{M}]_\gamma & [\mathbf{M}]_\delta \end{bmatrix}, \tag{23}$$

where each submatrix is $\frac{M}{2} \times \frac{M}{2}$ in size. Hereafter, we consider only the upper boundary processing. The signals at the lower boundary processing can be reconstructed in the same way as in the upper boundary processing.

1) Case of $K = 2$: From the top of Fig. 2, the middle signal $\mathbf{a}_0$ is expressed as

$$\mathbf{a}_0 = \begin{bmatrix} [\mathbf{X}_0]_\alpha & [\mathbf{X}_0]_\beta \end{bmatrix} \begin{bmatrix} \boldsymbol{\mathcal{E}}_{[\frac{M}{2}]} & \mathbf{O} \\ \mathbf{O} & \mathbf{I}_{[\frac{M}{2}]} \end{bmatrix} \begin{bmatrix} \mathbf{x}_0 \\ \mathbf{x}_0 \end{bmatrix} = \mathfrak{F}_0 \mathbf{x}_0, \tag{24}$$

where

$$\mathfrak{F}_0 = [\mathbf{X}_0]_\alpha \boldsymbol{\mathcal{E}}_{[\frac{M}{2}]} + [\mathbf{X}_0]_\beta \quad \text{s.t.} \quad |\det(\mathfrak{F}_0)| = d. \tag{25}$$

The problem in the synthesis banks is to reconstruct the input signal $\mathbf{x}_0$ from the middle signal $\mathbf{a}_0$, which is transmitted to the synthesis bank. The input signal $\mathbf{x}_0$ is represented as

$$\mathbf{x}_0 = \mathfrak{F}_0^{-1} \mathbf{a}_0. \tag{26}$$

The nonexpansive convolution of the FBs in case of $K = 2$ is shown at the bottom of Fig. 2.

2) Case of $K = 3$: From the top of Fig. 3, the middle signals $\mathbf{b}_{-1}$, $\mathbf{b}_0$, and $\mathbf{b}_1$ are expressed as

$$\mathbf{b}_{-1} = \begin{bmatrix} [\mathbf{X}_0]_\alpha & [\mathbf{X}_0]_\beta \end{bmatrix} \boldsymbol{\mathcal{E}}_{[M]} \begin{bmatrix} \mathbf{x}_0 \\ \mathbf{x}_1 \end{bmatrix} \tag{27}$$

$$\begin{bmatrix} \mathbf{b}_1 \\ \mathbf{b}_0 \end{bmatrix} = \mathbf{X}_0 \begin{bmatrix} \mathbf{x}_0 \\ \mathbf{x}_1 \end{bmatrix}. \tag{28}$$

By substituting

$$\begin{bmatrix}\mathbf{x}_0\\ \mathbf{x}_1\end{bmatrix} = \mathbf{X}_0^{-1}\begin{bmatrix}\mathbf{b}_1\\ \mathbf{b}_0\end{bmatrix}, \tag{29}$$

which is obtained from (28), into (27), the middle signal $\mathbf{b}_{-1}$ is represented as

$$\mathbf{b}_{-1} = \begin{bmatrix}[\mathbf{X}_0]_\alpha & [\mathbf{X}_0]_\beta\end{bmatrix}\boldsymbol{\mathcal{E}}_{[M]}\mathbf{X}_0^{-1}\begin{bmatrix}\mathbf{b}_1\\ \mathbf{b}_0\end{bmatrix} = \boldsymbol{\mathcal{F}}\mathbf{b}_0 + \boldsymbol{\mathcal{G}}\mathbf{b}_1, \tag{30}$$

where

$$\begin{aligned}\boldsymbol{\mathcal{F}} = &\left([\mathbf{X}_0]_\alpha\left[\boldsymbol{\mathcal{E}}_{[M]}\right]_\alpha + [\mathbf{X}_0]_\beta\left[\boldsymbol{\mathcal{E}}_{[M]}\right]_\gamma\right)\left[\mathbf{X}_0^{-1}\right]_\beta\\ &+\left([\mathbf{X}_0]_\alpha\left[\boldsymbol{\mathcal{E}}_{[M]}\right]_\beta + [\mathbf{X}_0]_\beta\left[\boldsymbol{\mathcal{E}}_{[M]}\right]_\delta\right)\left[\mathbf{X}_0^{-1}\right]_\delta \qquad (31)\\ \boldsymbol{\mathcal{G}} = &\left([\mathbf{X}_0]_\alpha\left[\boldsymbol{\mathcal{E}}_{[M]}\right]_\alpha + [\mathbf{X}_0]_\beta\left[\boldsymbol{\mathcal{E}}_{[M]}\right]_\gamma\right)\left[\mathbf{X}_0^{-1}\right]_\alpha\\ &+\left([\mathbf{X}_0]_\alpha\left[\boldsymbol{\mathcal{E}}_{[M]}\right]_\beta + [\mathbf{X}_0]_\beta\left[\boldsymbol{\mathcal{E}}_{[M]}\right]_\delta\right)\left[\mathbf{X}_0^{-1}\right]_\gamma. \qquad (32)\end{aligned}$$

Also, the middle signal $\mathbf{a}_0$ is expressed as

$$\mathbf{a}_0 = \begin{bmatrix}[\mathbf{X}_1]_\alpha & [\mathbf{X}_1]_\beta\end{bmatrix}\begin{bmatrix}\mathbf{b}_{-1}\\ \mathbf{b}_0\end{bmatrix} = [\mathbf{X}_1]_\alpha\mathbf{b}_{-1} + [\mathbf{X}_1]_\beta\mathbf{b}_0. \tag{33}$$

Substituting (30) into (33) yields

$$\mathbf{a}_0 = \mathfrak{F}_1\mathbf{b}_0 + \mathfrak{G}_1\mathbf{b}_1, \tag{34}$$

where

$$\mathfrak{F}_1 = [\mathbf{X}_1]_\alpha\boldsymbol{\mathcal{F}} + [\mathbf{X}_1]_\beta \quad \text{s.t.} \quad |\det(\mathfrak{F}_1)| = d \tag{35}$$

$$\mathfrak{G}_1 = [\mathbf{X}_1]_\alpha\boldsymbol{\mathcal{G}}. \tag{36}$$

Unlike the determinant of $\mathfrak{F}_1$, that of $\mathfrak{G}_1$ is not restricted to a natural number because the processing including $\mathfrak{G}_1$ can already be considered a lifting structure. The problem in the synthesis banks is to reconstruct the middle signal $\mathbf{b}_0$ from the middle signals $\mathbf{a}_0$ and $\mathbf{b}_1$, which is transmitted to the synthesis bank. The middle signal $\mathbf{b}_0$ is represented as

$$\mathbf{b}_0 = \mathfrak{F}_1^{-1}\left(\mathbf{a}_0 - \mathfrak{G}_1\mathbf{b}_1\right). \tag{37}$$

The nonexpansive convolution in the case of $K = 3$ is shown at the bottom of Fig. 3. For any K, the signals can be reconstructed as the solution of a simultaneous matrix equation with $(K-1)$ unknowns.

The new nonexpansive convolution can be used by all lifting-based FBs (not only ReBLFBs) having a lattice structure. In addition, the new part $\mathfrak{W}_k(z)$ of the ReBLFBs with longer synthesis filters than the analysis ones is skipped at the boundaries for simplicity.

C. Regularity for Redefined Block-Lifting-based Filter Banks

FB theory indicates that regularity, especially one degree of regularity (one-regularity), is an important property to prevent the DC leakage for image compression [29]. One-regularity in the ReBLFBs can be structurally imposed in the same way as in [27], because [29]

$$\left(\mathbf{E}(z)\begin{bmatrix}1\\ z^{-1}\\ \vdots\\ z^{-M}\end{bmatrix}\right)\Bigg|_{z=1} = \mathbf{E}_0\begin{bmatrix}1\\ 1\\ \vdots\\ 1\end{bmatrix} = \begin{bmatrix}c\\ 0\\ \vdots\\ 0\end{bmatrix}, \tag{38}$$

where $[1,1,\cdots,1]^\top$ are DC components, c is a nonzero constant, and any building block $\mathbf{E}_k(z)$ in the ReBLFB $\mathbf{E}(z)$ is skipped as follows:

$$\begin{aligned}\mathbf{E}_k(z)\big|_{z=1} &= \left(\mathfrak{L}_k^{-1}\mathfrak{W}_k(z)\mathfrak{U}_k\mathbf{\Lambda}_k(z)\mathfrak{U}_k^{-1}\mathfrak{L}_k\right)\big|_{z=1}\\ &= \mathfrak{L}_k^{-1}\mathbf{I}_{[M]}\mathfrak{U}_k\mathbf{I}_{[M]}\mathfrak{U}_k^{-1}\mathfrak{L}_k = \mathbf{I}_{[M]}. \qquad (39)\end{aligned}$$

Moreover, we must consider regularity in the proposed boundary processing. If the resulting ReBLFBs achieve structural one-regularity, we can also achieve it at the boundaries by preserving the DC components in the input signals; i.e., the extension matrix $\boldsymbol{\mathcal{E}}_{[L]}$ should be structurally restricted to

$$\boldsymbol{\mathcal{E}}_{[L]}\begin{bmatrix}1\\ 1\\ \vdots\\ 1\end{bmatrix} = \begin{bmatrix}1\\ 1\\ \vdots\\ 1\end{bmatrix}. \tag{40}$$

E.g., the extension matrix $\boldsymbol{\mathcal{E}}_{[L]}$ can be set as

$$\boldsymbol{\mathcal{E}}_{[L]} = \begin{bmatrix} e_{0,0} & \cdots & e_{0,L-2} & 1-\sum_{j=0}^{L-2} e_{0,j}\\ \vdots & \ddots & \vdots & \vdots\\ e_{L-2,0} & \cdots & e_{L-2,L-2} & 1-\sum_{j=0}^{L-2} e_{L-2,j}\\ e_{L-1,0} & \cdots & e_{L-1,L-2} & 1-\sum_{j=0}^{L-2} e_{L-1,j}\end{bmatrix}, \tag{41}$$

where $e_{i,j}$ $(i = 0,1,\cdots,L-1,\ j = 0,1,\cdots,L-2)$ is an arbitrary parameter.

D. Specific Filter Design

We specifically designed 4×8, $4\times 8/4\times 12$, and 4×12 ReBLFBs, which had $r_k = 2$ and structural one-regularity. The structures of 4×8 and 4×12 ReBLFBs are completely same as the conventional structures in [18]. We used the following cost function ϕ, which is a weighted linear combination of the coding gain [32], the determinant control of matrices, and the smoothness of the extension matrix $\boldsymbol{\mathcal{E}}_{[L]}$:

$$\phi = -w_0 C_{cg} + w_1 C_{det} + w_2 C_{smooth}, \tag{42}$$

where

$$C_{cg} = 10\log_{10}\frac{\frac{1}{M}\sum_{i=0}^{M-1}\sigma_i^2}{\left(\prod_{i=0}^{M-1}\sigma_i^2 f_i^2\right)^{\frac{1}{N}}} \tag{43}$$

$$C_{det} = \left(\left|\det\left(\mathfrak{F}_k^{\uparrow}\right)\right| - d\right)^2 + \left(\left|\det\left(\mathfrak{F}_k^{\downarrow}\right)\right| - d\right)^2 \tag{44}$$

$$\begin{aligned}C_{smooth} = \sum_{i=0}^{L-1}\sum_{j=0}^{L-1}\Bigg\{&\left(\left[\boldsymbol{\mathcal{E}}_{[L]}^{\uparrow}\right]_{ij} - \left[\boldsymbol{\mathcal{S}}_{[L]}\right]_{ij}\right)^2\\ &+\left(\left[\boldsymbol{\mathcal{E}}_{[L]}^{\downarrow}\right]_{ij} - \left[\boldsymbol{\mathcal{S}}_{[L]}\right]_{ij}\right)^2\Bigg\}, \qquad (45)\end{aligned}$$

TABLE I
CODING GAINS [DB].

	HLT	ReBLFBs		
	4×8	4×8	$4 \times 8/4 \times 12$	4×12
	[14]	same as [18]	new	same as [18]
C_{cg}[dB]	8.45	8.64	8.66	**8.79**

and `fminunc.m` in the `Optimization ToolBox` of `MATLAB`. σ_i^2 is the variance of the ith subband, and f_i^2 is the L_2 norm of the ith synthesis filter. When the transform has paraunitariness, the synthesis scaling f_i^2 drops out of the coding gain equation. The input signal is assumed to be an AR(1) model with autocorrelation coefficient $\rho = 0.95$ in common use. The super scripts $\uparrow$ and $\downarrow$ respectively mean the matrices at the upper and lower boundary processings of the FBs. $[\cdot]_{ij}$ means the (i,j)th element of a matrix. Since it is difficult to make $|\det(\mathfrak{F}_k)| = d$ exactly by using only the cost function C_{det}, which brings $|\det(\mathfrak{F}_k)|$ as close as possible to d, we used $\mathfrak{F}_k^{det}$, which is forcibly controlled,

$$\mathfrak{F}_k^{det} = \left(\frac{d}{|\det(\mathfrak{F}_k)|} \right)^{\frac{2}{M}} \mathfrak{F}_k \tag{46}$$

instead of $\mathfrak{F}_k$, where we set $d = 1$ for simplicity. The cost function C_{det} should be imposed because the boundary processing cannot be implemented smoothly when $|\det(\mathfrak{F}_k)|$ is substantially different from d, i.e., $\mathfrak{F}_k^{det}$ is substantially different from $\mathfrak{F}_k$. For example, $|\det(\mathfrak{F}_k^{\uparrow})|$ in the resulting $4 \times 8/4 \times 12$ ReBLFB was $0.92 \approx 1$. In addition, we set the smoothness condition as a symmetric extension $\boldsymbol{\mathcal{S}}_{[L]} = \mathbf{J}_{[L]}$. The weights w_k $(k = 0, 1, 2)$ are heuristically determined because the resulting filter coefficients may lead to a local minimum, and this is due to depense of the solution on the initial values and the weights.

IV. EXPERIMENTAL RESULTS

A. Coding Gain and Frequency/Impulse Responses

Table I shows the coding gains C_{cg} of the HLT [14] in JPEG XR and the resulting ReBLFBs. We can see that the ReBLFBs have higher coding gains than that of the HLT restricted by the LP property and the ReBLFBs with longer filter lengths have higher coding gains than those with shorter filter lengths.

Fig. 4 shows frequency and impulse responses of the resulting ReBLFBs. Those of $4 \times 8/4 \times 12$ ReBLFB resembles those of 4×8 ReBLFB in appearance because the difference in structure is trivial; i.e., $\boldsymbol{\mathcal{W}}_1 = \mathbf{I}_{[\frac{M}{2}]}$ or $\boldsymbol{\mathcal{W}}_1 \neq \mathbf{I}_{[\frac{M}{2}]}$. However, it is clear that unlike the others, the $4 \times 8/4 \times 12$ ReBLFB has longer synthesis filter lengths than the analysis filter lengths.

B. Lossy-to-Lossless Image Coding

The resulting ReBLFBs were implemented with a rounding operation at each lifting step and compared in terms of the lossless bitrate (LBR) [bpp]:

$$\text{LBR [bpp]} = \frac{\text{Total number of bits [bit]}}{\text{Total number of pixels [pixel]}}$$

TABLE II
LOSSLESS IMAGE CODING RESULTS (LBR [BPP]; () IS IN A PERIODIC EXTENSION).

Test	HLT	ReBLFBs		
Images	4×8	4×8	$4 \times 8/4 \times 12$	4×12
	[14]	same as [18]	new	same as [18]
Bike	5.26	5.18 (5.19)	**5.16** (5.17)	**5.16** (5.17)
Building	4.17	4.17 (4.18)	**4.12** (4.13)	4.14 (4.15)
Cafe	6.09	6.04 (6.05)	6.03 (6.04)	**6.02** (6.03)
Car	4.10	4.10 (4.11)	**4.07** (4.08)	4.11 (4.13)
Falls	4.18	4.17 (4.19)	**4.12** (4.14)	4.14 (4.15)
Flower	4.44	4.40 (4.41)	**4.39** (4.40)	4.42 (4.42)
Girl	4.37	4.39 (4.40)	**4.34** (4.35)	4.36 (4.37)
House	4.94	4.93 (4.94)	**4.87** (4.88)	4.88 (4.90)
Sakura	4.48	4.41 (4.42)	**4.39** (4.40)	4.42 (4.43)
Woman	4.86	4.83 (4.85)	**4.81** (4.83)	4.83 (4.84)
r0ebb0bb4t	4.64	4.58 (4.58)	**4.55** (4.56)	4.56 (4.56)
r0ed019a4t	3.27	3.33 (3.34)	**3.24** (**3.24**)	3.27 (3.28)
r0f24ca4dt	4.65	4.58 (4.59)	4.53 (4.53)	**4.52** (4.53)
r0fb0a690t	4.35	4.30 (4.30)	**4.26** (4.27)	4.28 (4.28)
r02d732f8t	3.83	3.85 (3.85)	**3.78** (3.79)	3.80 (3.80)
r03b0c944t	4.70	4.61 (4.61)	**4.58** (**4.58**)	4.59 (4.59)
r08f2d4c6t	3.92	3.94 (3.95)	**3.90** (3.91)	3.92 (3.92)
r069e346et	3.70	3.73 (3.73)	**3.68** (3.69)	3.71 (3.72)
r0773471dt	5.11	5.02 (5.02)	5.00 (5.00)	**4.99** (**4.99**)
r01170470t	3.96	3.96 (3.97)	**3.86** (3.87)	3.87 (3.88)
mLBR	4.06	4.01 (4.02)	**3.96** (3.97)	3.99 (3.99)
SD	0.71	0.70 (0.70)	0.71 (0.71)	0.70 (0.70)

in lossless image coding and in terms of the peak signal-to-noise ratio (PSNR) [dB]:

$$\text{PSNR [dB]} = 10 \log_{10} \left(\frac{\left(2^{\text{BIT}} - 1\right)^2}{\text{MSE}} \right),$$

where BIT and MSE are the number of bits of the image and the mean squared error, and multi-scale structural similarity (MS-SSIM) [35], which is an image quality assessment based on human visual characteristics unlike PSNR, in lossy image coding. To evaluate the transform performance fairly, we employed three-level decompositions on all filters. The image set included 1024×1024 and 2048×2048 clipped 8-bit standard grayscale images in [33], [34] (see Fig. 5). Also, in addition to the results of images in Fig. 5, the mean LBR (mLBR), mean PSNR (mPSNR), mean MS-SSIM (mMS-SSIM), and standard deviation (SD) of the other 100 images in [34] are shown. A quadtree-based embedded image coder [36], which is more suited to block transforms than are the popular zerotree-based coders [37], [38], was used to encode the transformed images.

Tables II-IV and Fig. 6 show the results of lossless and lossy image coding. Although the HLT, 4×8 ReBLFB, and 4×12 ReBLFB sometimes performed the best, the $4 \times 8/4 \times 12$ ReBLFB basically outperformed the others. In addition, the $4 \times 8/4 \times 12$ ReBLFB avoided ringing artifacts around regions with high-frequency components as well as blocking artifacts around regions with low-frequency components and the proposed nonexpansive convolution helped to inhibit the boundary artifacts.

V. CONCLUSION

This study redefined a block-lifting structure of M-channel FBs and proposed an efficient reversible nonexpansive convolution for lossy-to-lossless image coding. We solved two

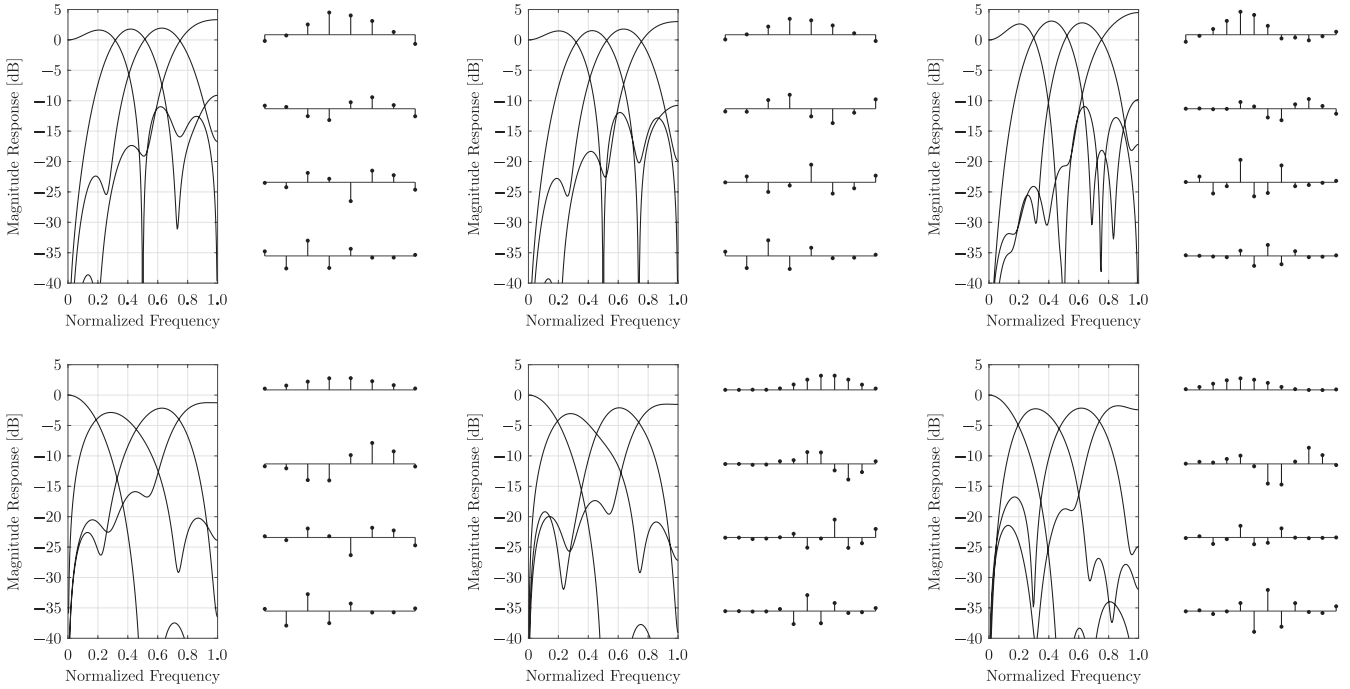

Fig. 4. Frequency and impulse responses of the ReBLFBs: (top) analysis bank, (bottom) synthesis bank, (left) 4×8, (middle) $4 \times 8/4 \times 12$, and (right) 4×12.

problems, i.e., the restriction of equal analysis/synthesis filter lengths and lack of an efficient reversible nonexpansive convolution, left by our previous work. We showed that the ReBLFBs with the nonexpansive convolution performed well at lossy-to-lossless image coding.

ACKNOWLEDGMENT

The authors would like to thank the anonymous reviewers for providing many constructive suggestions that significantly improve the presentation of this paper. This work was supported by JSPS Grant-in-Aid for Young Scientists (B), Grant Number 16K18100.

REFERENCES

[1] A. Skodras, C. Christopoulis, and T. Ebrahimi, "The JPEG2000 still image compression standard," *IEEE Signal Process. Mag.*, vol. 18, no. 5, pp. 36–58, Sep. 2001.

[2] F. Dufaux, G. J. Sullivan, and T. Ebrahimi, "The JPEG XR image coding standard," *IEEE Signal Process. Mag.*, vol. 26, no. 6, pp. 195–199, 204, Nov. 2009.

[3] G. Toderici, D. Vincent, N. Johnston, S. J. Hwang, D. Minnen, J. Shor, and M. Covell, "Full resolution image compression with recurrent neural networks," in *Proc. of CVPR'17*, Honolulu, HI, July 2017, pp. 5306–5314.

[4] O. Rippel and L. Bourdev, "Real-time adaptive image compression," in *Proc. of ICML'17*, Sydney, Australia, Aug. 2017, pp. 2922–2930.

[5] W. Sweldens, "The lifting scheme: A construction of second generation wavelets," *SIAM J. Math. Anal.*, vol. 29, no. 2, pp. 511–546, 1998.

[6] T. Yoshida, T. Suzuki, S. Kyochi, and M. Ikehara, "Two dimensional non-separable adaptive directional lifting structure of discrete wavelet transform," *IEICE Trans. Fundamentals.*, vol. E94-A, no. 10, pp. 1920–1927, Oct. 2011.

[7] M. Iwahashi and H. Kiya, "Reversible 2D 9-7 DWT based on non-separable 2D lifting structure compatible with irreversible DWT," *IEICE Trans. Fundamentals.*, vol. E94-A, no. 10, pp. 1928–1936, Oct. 2011.

[8] T. Strutz and I. Rennert, "Two-dimensional integer wavelet transform with reduced influence of rounding operations," *EURASIP J. Adv. Signal Process.*, vol. 2012, no. 75, pp. 1–18, Dec. 2012.

[9] T. Orachon, T. Yoshida, M. Iwahashi, and H. Kiya, "Channel scaling for integer implementation of minimum lifting 2D wavelet transform," *IEICE Trans. Fundamentals.*, vol. E99-A, no. 7, pp. 1420–1429, July 2016.

[10] P. Hao and Q. Shi, "Matrix factorizations for reversible integer mapping," *IEEE Trans. Signal Process.*, vol. 49, no. 10, pp. 2314–2324, Oct. 2001.

[11] T. D. Tran, J. Liang, and C. Tu, "Lapped transform via time-domain pre- and post-filtering," *IEEE Trans. Signal Process.*, vol. 6, no. 6, pp. 1557–1571, June 2003.

[12] Y. J. Chen and K. S. Amaratunga, "M-channel lifting factorization of perfect reconstruction filter banks and reversible M-band wavelet transforms," *IEEE Trans. Circuits Syst. II*, vol. 50, no. 12, pp. 963–976, Dec. 2003.

[13] Y. She, P. Hao, and Y. Paker, "Matrix factorizations for parallel integer transformation," *IEEE Trans. Signal Process.*, vol. 54, no. 12, pp. 4675–4684, Dec. 2006.

[14] C. Tu, S. Srinivasan, G. J. Sullivan, S. Regunathan, and H. S. Malvar, "Low-complexity hierarchical lapped transform for lossy-to-lossless image coding in JPEG XR/HD Photo," in *Proc. of SPIE*, vol. 7073, San Diego, CA, Aug. 2008, pp. 70 730C–1–70 730C–12.

[15] C. M. Brislawn, "Group lifting structures for multirate filter banks I: Uniqueness of lifting factorizations," *IEEE Trans. Signal Process.*, vol. 58, no. 4, pp. 2068–2077, Apr. 2010.

[16] ——, "Group lifting structures for multirate filter banks II: Linear phase filter banks," *IEEE Trans. Signal Process.*, vol. 58, no. 4, pp. 2078–2087, Apr. 2010.

[17] S. Iwamura, Y. Tanaka, and M. Ikehara, "An efficient lifting structure of biorthogonal filter banks for lossless image coding," in *Proc. of ICIP'07*, San Antonio, TX, Sep. 2007, pp. 433–436.

[18] T. Suzuki, M. Ikehara, and T. Q. Nguyen, "Generalized block-lifting factorization of M-channel biorthogonal filter banks for lossy-to-lossless image coding," *IEEE Trans. Image Process.*, vol. 21, no. 7, pp. 3220–3228, July 2012.

[19] T. Suzuki and H. Kudo, "2D non-separable block-lifting structure and its application to M-channel perfect reconstruction filter banks for lossy-to-lossless image coding," *IEEE Trans. Image Process.*, vol. 24, no. 12, pp. 4943–4951, Dec. 2015.

[20] X. Song, Q. Huang, S. Chang, J. He, and H. Wang, "Three-dimensional

Fig. 5. Test images excerpted from data set: (top) *Bike*, *Building*, *Cafe*, *Car*, *Falls*, *Flower*, *Girl*, *House*, *Sakura*, and *Woman* in [33], (middle and bottom) *r0ebb0bb4t*, *r0ed019a4t*, *r0f24ca4dt*, *r0fb0a690t*, *r02d732f8t*, *r03b0c944t*, *r08f2d4c6t*, *r069e346et*, *r0773471dt*, and *r01170470t* in [34].

Fig. 6. Comparison of results in a particular area of the image *Cafe* (top and left sides are boundaries; bitrate: 0.25 [bpp]): (top-left) original image, (other left-to-right) 4×8 HLT, 4×8 ReBLFB, $4 \times 8/4 \times 12$ ReBLFB, and 4×12 ReBLFB, (top) a periodic extension, and (bottom) the proposed nonexpansive convolution.

separate descendant-based SPIHT algorithm for fast compression of high-resolution medical image sequences," *IET Image Process.*, vol. 11, no. 1, pp. 80–87, Jan. 2017.

[21] F. A. B. Hamzah, T. Yoshida, and M. Iwahashi, "Non-separable quadruple lifting structure for four-dimensional integer wavelet transform with reduced rounding noise," in *Proc. of ICASSP'17*, New Orleans, LA, Mar. 2017, pp. 1148–1152.

[22] S. Álvarez-Cortès, N. Amrani, M. Hernández-Cabronero, and J. Serra-Sagristà, "Progressive lossy-to-lossless coding of hyperspectral images through regression wavelet analysis," *Int. J. Remote Sens.*, pp. 1–21, Jun. 2017.

[23] Y. Tanaka, M. Ikehara, and T. Q. Nguyen, "A simplified lattice structure of first-order linear-phase filter banks," in *Proc. of EUSIPCO'07*, Poznań, Poland, Sep. 2007, pp. 55–59.

[24] T. Suzuki and M. Ikehara, "Reversible symmetric non-expansive convolution: An effective image boundary processing for M-channel lifting-based linear-phase filter banks," *IEEE Trans. Image Process.*, vol. 23, no. 6, pp. 2744–2749, June 2014.

[25] M. J. T. Smith and S. L. Eddins, "Analysis/synthesis techniques for subband image coding," *IEEE Trans. Signal Process.*, vol. 38, no. 8, pp. 1446–1456, Aug. 1990.

[26] Y. Tanaka, A. Ochi, and M. Ikehara, "A non-expansive convolution for nonlinear-phase paraunitary filter banks and its application to image coding," in *Proc. of ACSSC'05*, Pacific Grove, CA, Oct. 2005, pp. 54–58.

[27] T. Uto, T. Oka, and M. Ikehara, "M-channel nonlinear phase filter banks in image compression: Structure, design, and signal extension," *IEEE Trans. Signal Process.*, vol. 55, no. 4, pp. 1339–1351, Apr. 2007.

[28] T. Suzuki, N. Tanaka, and H. Kudo, "Pseudo reversible symmetric extension for lifting-based nonlinear-phase paraunitary filter banks," in *Proc. of ICIP'17*, Beijing, China, Sep. 2017, pp. 3265–3269.

[29] Y. J. Chen, S. Oraintara, and K. S. Amaratunga, "Theory and factorization for a class of structurally regular biorthogonal filter banks," *IEEE Trans. Signal Process.*, vol. 54, no. 2, pp. 691–700, Feb. 2006.

[30] P. P. Vaidyanathan and T. Chen, "Role of anticausal inverses in multirate filter-banks–part II: The FIR case, factorizations, and biorthogonal lapped transforms," *IEEE Trans. Signal Process.*, vol. 43, no. 5, pp. 1103–1115, May 1995.

[31] Y. Tanaka, M. Ikehara, and T. Q. Nguyen, "A lattice structure of biorthogonal linear-phase filter banks with higher order feasible building blocks," *IEEE Trans. Circuits Syst. I*, vol. 55, no. 8, pp. 2322–2331, Sep.

TABLE III
LOSSY IMAGE CODING RESULTS (PSNR [DB]; () IS IN A PERIODIC EXTENSION).

Bitrate [bpp]	HLT 4×8 [14]	ReBLFBs 4×8 same as [18]	$4\times8/4\times12$ new	4×12 same as [18]
		Bike		
0.25	**24.52**	24.26 (24.19)	24.48 (24.44)	24.35 (24.37)
0.50	28.16	28.16 (28.10)	**28.35** (28.28)	28.20 (28.21)
1.00	33.22	33.50 (33.49)	**33.73** (33.72)	33.57 (33.56)
		Cafe		
0.25	20.16	20.32 (20.31)	**20.45** (**20.45**)	20.16 (20.19)
0.50	23.02	23.20 (23.18)	**23.39** (**23.39**)	22.93 (22.94)
1.00	26.97	27.19 (27.15)	**27.41** (27.38)	27.09 (27.07)
		Falls		
0.25	31.30	31.34 (30.91)	**31.39** (30.98)	31.03 (30.79)
0.50	34.66	34.93 (34.56)	**35.12** (34.70)	34.42 (34.26)
1.00	38.85	39.03 (38.97)	**39.42** (39.35)	39.29 (39.22)
		Girl		
0.25	33.75	34.11 (33.94)	**34.27** (34.12)	34.17 (33.97)
0.50	36.30	36.51 (36.41)	**36.74** (36.63)	36.59 (36.48)
1.00	39.23	39.07 (39.02)	**39.46** (39.40)	39.23 (39.17)
		Sakura		
0.25	28.05	28.84 (28.79)	29.03 (28.98)	**29.12** (**29.12**)
0.50	31.75	32.64 (32.62)	32.89 (32.85)	32.89 (**32.90**)
1.00	37.00	37.25 (37.12)	**37.55** (37.43)	37.22 (37.18)
		r0ebb0bb4t		
0.25	28.54	28.77 (28.72)	28.88 (28.82)	**28.91** (28.86)
0.50	31.63	32.05 (32.04)	32.25 (32.24)	**32.33** (32.29)
1.00	35.38	35.92 (35.92)	36.23 (36.23)	**36.28** (36.26)
		r0f24ca4dt		
0.25	27.36	27.47 (27.42)	**27.65** (27.60)	27.63 (27.57)
0.50	30.63	30.95 (30.93)	**31.22** (31.18)	31.14 (31.11)
1.00	34.71	35.29 (35.25)	**35.60** (35.59)	35.52 (35.49)
		r02d732f8t		
0.25	33.05	33.33 (33.32)	**33.58** (33.53)	33.51 (33.43)
0.50	37.07	37.50 (37.53)	37.83 (**37.85**)	37.72 (37.67)
1.00	41.22	41.13 (41.14)	41.55 (**41.56**)	41.49 (41.48)
		r08f2d4c6t		
0.25	34.07	34.40 (34.33)	**34.60** (34.53)	34.49 (34.45)
0.50	37.40	37.72 (37.71)	**37.96** (37.94)	37.90 (37.87)
1.00	40.95	40.85 (40.84)	**41.29** (**41.29**)	41.26 (41.24)
		r0773471dt		
0.25	27.24	27.17 (27.15)	**27.27** (27.25)	**27.27** (27.25)
0.50	30.10	29.99 (29.97)	30.12 (30.11)	**30.17** (30.16)
1.00	33.46	33.53 (33.53)	**33.85** (33.84)	33.82 (33.83)
		mPSNR		
0.25	32.95	32.92 (32.87)	**33.10** (33.04)	33.02 (32.95)
0.50	35.93	35.89 (35.85)	**36.16** (36.12)	36.05 (36.00)
1.00	39.24	39.09 (39.07)	**39.62** (39.60)	39.44 (39.41)
		SD		
0.25	5.69	5.59 (5.60)	5.62 (5.63)	5.66 (5.65)
0.50	5.16	4.91 (4.93)	5.03 (5.05)	5.08 (5.08)
1.00	4.42	3.85 (3.86)	4.09 (4.10)	4.14 (4.14)

TABLE IV
LOSSY IMAGE CODING RESULTS (MS-SSIM; () IS IN A PERIODIC EXTENSION).

Bitrate [bpp]	HLT 4×8 [14]	ReBLFBs 4×8 same as [18]	$4\times8/4\times12$ new	4×12 same as [18]
		Bike		
0.25	0.892	0.910 (0.910)	**0.914** (0.913)	0.901 (0.901)
0.50	0.944	0.953 (0.953)	**0.955** (**0.955**)	0.951 (0.951)
1.00	0.977	0.981 (0.981)	**0.982** (**0.982**)	0.980 (0.980)
		Cafe		
0.25	0.869	0.880 (0.879)	**0.884** (**0.884**)	0.862 (0.861)
0.50	0.923	0.934 (0.934)	**0.937** (0.936)	0.924 (0.922)
1.00	0.962	0.969 (0.969)	**0.970** (**0.970**)	0.966 (0.965)
		Falls		
0.25	0.945	**0.951** (0.945)	**0.951** (0.947)	0.944 (0.942)
0.50	0.977	0.980 (0.978)	**0.981** (0.978)	0.975 (0.974)
1.00	0.991	0.992 (0.992)	**0.993** (**0.993**)	0.992 (0.992)
		Girl		
0.25	0.961	0.966 (0.965)	**0.968** (0.966)	0.963 (0.962)
0.50	0.979	0.982 (0.981)	**0.983** (0.982)	0.980 (0.979)
1.00	0.990	0.990 (0.990)	**0.991** (**0.991**)	0.990 (0.990)
		Sakura		
0.25	0.954	0.965 (0.964)	**0.966** (**0.966**)	0.964 (0.964)
0.50	0.980	0.985 (0.985)	**0.986** (**0.986**)	0.985 (0.985)
1.00	0.994	0.994 (0.994)	**0.995** (**0.995**)	0.994 (0.994)
		r0ebb0bb4t		
0.25	0.937	0.947 (0.946)	**0.948** (0.947)	0.938 (0.938)
0.50	0.969	0.975 (0.975)	**0.977** (0.976)	0.974 (0.973)
1.00	0.987	0.989 (0.989)	**0.990** (**0.990**)	0.989 (0.989)
		r0f24ca4dt		
0.25	0.932	0.939 (0.938)	**0.940** (0.939)	0.930 (0.930)
0.50	0.969	0.973 (0.973)	**0.974** (**0.974**)	0.969 (0.969)
1.00	0.987	0.990 (0.990)	**0.991** (**0.991**)	0.990 (0.989)
		r02d732f8t		
0.25	0.981	0.982 (0.982)	**0.983** (0.982)	0.981 (0.980)
0.50	0.990	**0.991** (**0.991**)	**0.991** (**0.991**)	**0.991** (**0.991**)
1.00	0.994	0.994 (0.994)	**0.995** (**0.995**)	**0.995** (**0.995**)
		r08f2d4c6t		
0.25	0.968	0.972 (0.972)	**0.973** (**0.973**)	0.969 (0.968)
0.50	0.985	0.987 (0.987)	**0.988** (**0.988**)	0.986 (0.986)
1.00	0.993	0.993 (0.993)	**0.994** (**0.994**)	**0.994** (**0.994**)
		r0773471dt		
0.25	0.890	0.899 (0.899)	**0.902** (**0.902**)	0.884 (0.884)
0.50	0.953	0.953 (0.953)	**0.955** (0.954)	0.945 (0.945)
1.00	0.981	0.983 (0.983)	**0.984** (**0.984**)	0.981 (0.980)
		mMS-SSIM		
0.25	0.958	0.961 (0.960)	**0.962** (**0.962**)	0.956 (0.956)
0.50	0.980	0.981 (0.981)	**0.982** (**0.982**)	0.979 (0.979)
1.00	0.991	0.991 (0.991)	**0.993** (0.992)	0.991 (0.991)
		SD		
0.25	0.028	0.026 (0.026)	0.025 (0.025)	0.030 (0.030)
0.50	0.014	0.013 (0.013)	0.012 (0.012)	0.015 (0.015)
1.00	0.006	0.005 (0.005)	0.005 (0.005)	0.006 (0.006)

2008.

[32] P. P. Vaidyanathan, *Multirate Systems and Filter Banks*. Englewood Cliffs, NJ: Prentice Hall, 1992.

[33] "JPEG core experiment for the evaluation of JPEG XR image coding," *EPFL, Multimedia Signal Processing Group [Online]*, Available: http://mmspg.epfl.ch/iqa.

[34] D.-T. Dang-Nguyen, C. Pasquini, V. Conotter, and G. Boato, "RAISE - a raw images dataset for digital image forensics," in *Proc. of MMSys'15*, Portland, OR, Mar. 2015, pp. 219–224.

[35] Z. Wang, E. P. Simoncelli, and A. C. Bovik, "Multi-scale structural similarity for image quality assessment," in *Proc. of ACSSC'03*, Pacific Grove, CA, Nov. 2003, pp. 1–5.

[36] Z. Liu and L. J. Karam, "An efficient embedded zerotree wavelet image codec based on intraband partitioning," in *Proc. of ICIP'00*, Vancouver, British Columbia, Canada, Sep. 2000, pp. 162–165.

[37] J. M. Shapiro, "Embedded image coding using zerotrees of wavelet coefficients," *IEEE Trans. Signal Process.*, vol. 41, no. 12, pp. 3445–3462, Dec. 1993.

[38] A. Said and W. A. Pearlman, "A new, fast, and efficient image codec based on set partitioning in hierarchical trees," *IEEE Trans. Circuits Syst. Video Technol.*, vol. 6, no. 3, pp. 243–250, June 1996.

Taizo Suzuki (S'08-M'11-SM'17) received the B.E., M.E., and Ph.D. degrees in electrical engineering from Keio University, Japan, in 2004, 2006 and 2010, respectively. From 2006 to 2008, he was with Toppan Printing Co., Ltd., Japan. From 2008 to 2011, he was a Research Associate of the Global Center of Excellence (G-COE) at Keio University, Japan. From 2010 to 2011, he was a Research Fellow of the Japan Society for the Promotion of Science (JSPS) and a Visiting Scholar at the Video Processing Group, the University of California, San Diego, CA. From 2011 to 2012, he was an Assistant Professor in the Department of Electrical and Electronic Engineering, College of Engineering, Nihon University, Japan. Since 2012, he has been an Assistant Professor in the Faculty of Engineering, Information and Systems, University of Tsukuba, Japan. His current research interests are image and video processing, source coding, and multidimensional transforms. Since 2017, he has been an Associate Editor of IEICE Trans. Fundamentals.

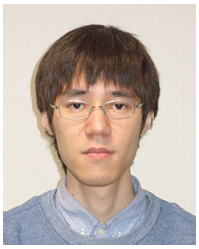

Naoki Tanaka received the B.E. and M.E. degrees from the University of Tsukuba, Japan, in 2015 and 2017, respectively. In 2017, he joined Sony LSI Design Inc., Japan. His research interests are signal/image processing and integrated circuit design.

Hiroyuki Kudo (M'88) received the B.Sc. degree from the Department of Electrical Communications, Tohoku University, Japan, in 1985, and the Ph.D. degree from the Graduate School of Engineering, Tohoku University, in 1990. In 1992, he joined the University of Tsukuba, Japan, as an Assistant Professor. He is currently a Professor with the Division of Information Engineering, Faculty of Engineering, Information and Systems, University of Tsukuba, Japan. He is involved in tomographic image reconstruction for X-ray CT, PET, SPECT, and electron tomography. His research areas include medical imaging, image processing, and inverse problems. He is a member of the Japanese Society of Medical Imaging Technology and IEICE, Japan. He received the best paper award several times from various domestic and international academic societies. In particular, his papers on interior tomography published in 2008 were selected as High Lights of the two journals, Physics in Medicine and Biology and Inverse Problems. Since 2011, he has been an Editor-in-Chief of the Journal of Medical Imaging Technology at MIT.